A Photo-Chemical Method for the Production of Olivine Nanoparticles as Cosmic Dust Analogues

Russell W. Saunders, John M.C. Plane

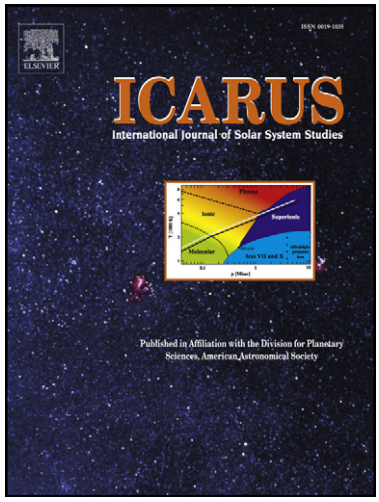

A Photo-Chemical Method for the Production of Olivine Nanoparticles as Cosmic Dust Analogues

Russell W. Saunders, John M.C. Plane

PII: S0019-1035(10)00487-2
DOI: 10.1016/j.icarus.2010.12.019
Reference: YICAR 9670

To appear in: *Icarus*

Received Date: 16 August 2010
Revised Date: 24 November 2010
Accepted Date: 18 December 2010

Please cite this article as: Saunders, R.W., Plane, J.M.C., A Photo-Chemical Method for the Production of Olivine Nanoparticles as Cosmic Dust Analogues, *Icarus* (2010), doi: 10.1016/j.icarus.2010.12.019

A Photo-Chemical Method for the Production of Olivine Nanoparticles as Cosmic Dust Analogues

Russell W. Saunders and John M.C. Plane

School of Chemistry, University of Leeds, Leeds UK LS2 9JT

Corresponding author: John Plane - email: j.m.c.plane@leeds.ac.uk/Tel: +44 (0)113 38044/Fax: +44 (0)113 3436565

Abstract

This paper describes a new experimental method to synthesise metal silicate particles in the laboratory with compositions and structures which reflect those likely to form in planetary atmospheres and in relatively cool regions of oxygen-rich stellar outflows. Fe-Mg-silicate nanoparticles of olivine composition were produced by the photo-oxidation of a mixture of $Fe(CO)_5$, $Mg(OC_2H_5)_2$ and $Si(OC_2H_5)_4$ vapours in the presence of O_3 at room temperature and atmospheric pressure. Transmission electron microscope x-ray and electron energy loss analysis of the particles from a number of experiments run with different precursor vapour mixture ratios show that $Mg_{2x}Fe_{2-2x}SiO_4$ particles can be produced ranging from $x = 0$ to 1, where x is linearly proportional to the ratio of $Mg(OC_2H_5)_2$ / ($Fe(CO)_5$ + $Mg(OC_2H_5)_2$). Electronic structure calculations with hybrid density functional/Hartree-Fock theory are then used to explore the pathways involved in producing olivine particles from the FeO_3, MgO_3 and SiO_2 produced from the photolysis of the organometallic precursors in O_3. These calculations indicate that highly exothermic reactions lead to the formation of Mg_2SiO_4, $MgFeSiO_4$ and Fe_2SiO_4 molecules, which

then polymerize. An alternative pathway, also strongly favoured thermodynamically, is the polymerization of $MgSiO_3$ and $FeSiO_3$ to form pyroxenes, which then undergo structural rearrangement to olivine and silica phases. The implications for metal silicate formation in planetary atmosphere and stellar outflows are then discussed.

1. Introduction

Speculation on the chemical composition of dust particles found in a variety of extra-terrestrial environments (e.g. interstellar and circumstellar), backed by the large database of optical measurements made over the past half century or so (see Whittet, 2003), invariably identifies metal (primarily iron and magnesium) silicate compounds as a major component (Rietmeijer, 2002; Draine, 2003; Henning, 2010). Indeed, the term 'astronomical silicate' has been coined for a general olivine ($Mg_{2x}Fe_{2-2x}SiO_4$; $x \sim 0.5$) structure which provides a best-fit to certain features in the optical data (Draine and Lee, 1984). These dust particles are not only important in that they scatter, absorb and re-radiate light, but also because they act as catalytic substrates for the uptake and reaction of ambient gas-phase species, and hence are thought to be vital for the synthesis of detected molecular species such as H_2 and CO (Williams and Taylor, 1996).

Analysis of peak structure within the diagnostic Si-O bond vibrations at ~ 10 and 18 microns suggests a crystalline, Mg-rich ($x > 0.5$) nature for these mineral forms (pyroxene and olivine) of dust in certain high temperature environments i.e. in proximity to evolving stars (Gail and Sedlmayr, 1999) and also in comets and planetary nebulae (Jäger et al. 1998). However, it has been reported that amorphous Fe-rich ($x < 0.5$) olivine variations are dominant in the interstellar medium or ISM (Draine, 2003; Kemper et al.,

2004), with a significant proportion of such grains in the lowest density regions of the ISM being less than 3 nm in size (Li and Draine, 2001).

It has long been suggested that nanoparticles of 'meteoric smoke' are formed in the upper atmosphere of the Earth, as a result of meteor ablation and subsequent condensation of gas-phase metal oxide and silicate species (Rosinski and Snow, 1961; Hunten et al., 1980). Ablation modelling indicates that the majority of atoms/ions released into the atmosphere from the parent meteoroid are (in approximately equivalent amounts) those of iron, magnesium and silicon (Vondrak et al., 2008). Subsequent oxidation of these species is then likely to initiate condensation of solid-phase silicaceous material (smoke particles).

Such particles are predicted to be of the order of only a few nanometres in size and consequently, proof of their existence through optical methods has to date been difficult and largely inconclusive. Recent satellite-bound spectrometer measurements of high altitude particle extinction seem to be the first to identify these tiny smoke particles (Hervig et al., 2009), although compositional fitting of such data is reliant on refractive index data available for a limited range of silicate materials prepared in the laboratory.

The interaction of meteoric smoke particles or MSPs with gases such as H_2O and H_2SO_4 in the Earth's atmosphere has long been thought to play a role in such phenomena as high altitude ice particle nucleation, leading to the related phenomena of noctilucent clouds and polar mesosphere summer echoes (Rapp and Thomas, 2006), and the depletion of acidic gases in the upper stratosphere (Turco et al., 1981). Clearly the precise nature of such particle-vapour interactions will be strongly dependent on the particle composition. The formation of meteoric smoke (and subsequent interaction with organic vapours) has

recently been postulated to account for the observed 'detached' aerosol layer in Titan's atmosphere (Lavvas et al., 2009). MSPs are also almost certainly the nuclei which form CO_2-ice clouds in the Mars mesosphere around 80 km (Montmessin et al., 2006). In the ISM, dust particles play a crucial role, for example, in the synthesis of molecules through heterogeneous chemistry (e.g. Williams and Hartquist, 1999).

The critical ingredients for the formation of such smoke and dust particles in the terrestrial and other planetary atmospheres, and in favourable regions of the ISM (see the review of Henning, 2010) such as, for example, the cooling outflows / circumstellar envelopes of oxygen-rich asymptotic giant branch (AGB) stars (e.g. Gail and Sedlmayr, 1999; Gail, 2010), planetary nebulae (e.g. Gorny et al., 2010) or regions chemically enriched by supernovae (e.g. Kotak et al., 2009), are (i) a source of metal and silicon atoms, and (ii) an oxidising species to form the initial gas-phase metal oxide and silicon oxide molecules. These can then react to form molecular silicate species (see section 3.2). In planetary/satellite atmospheres where the atmospheric pressure is greater than about 1 μbar, meteoric ablation occurs (e.g. McAuliffe and Christou, 2006; Kim et al., 2001; Ip, 1990; English et al., 1996; Molina-Cuberos et al., 2008; Pesnell and Grebowsky, 2000; Whalley and Plane, 2010). The resulting metal and silicon atoms are then oxidized in the presence of O_3 and O_2, which tend to be present at some level (e.g. Fast et al., 2009; Migliorini et al., 2010; Noll et al., 1997; Hörst et al., 2008). In the ISM, the stellar nucleosynthesis and ejection of metals such as Fe and Mg and of Si accompanied by the presence of oxygen in the form of neutral and ionised forms or in volatile molecules or ices (Jensen et al., 2008) will likewise be conducive to the formation of silicate species.

The production of analogue materials for cosmic dust studies has utilised a number of methods (reviewed by Colangeli et al., 2003) including room temperature sol-gel preparations (Thompson et al., 1996; Jäger et al., 2003), melt quenching (Dorschner et al., 1995), and vapour condensation methods such as laser ablation-condensation (Brucato et al., 2002) and high temperature evaporation-condensation (Rietmeijer et al., 1999; Nuth et al., 2000). The purpose of such laboratory techniques is not to replicate directly the chemical or physical conditions in which particle formation can occur in the Earth's atmosphere, other planetary atmospheres or the ISM, but to provide a way of forming particles of realistic composition and structure for the subsequent study of their physical and chemical properties under conditions appropriate for a targeted environment.

Sol-gel/melt quenching syntheses can produce amorphous pyroxene and olivine compounds with mixed compositions, but the vapour condensation methods to date have indicated that formation of mixed Mg-Fe silicate materials is not favoured. However, more recent studies using the photo-oxidation of 'binary' mixtures of iron and silicon precursor vapours at room temperature (Saunders and Plane, 2006; Kimura and Nuth, 2007) led to the preferential nucleation and subsequent growth of amorphous particles with end-member olivine composition. To the best of our knowledge, there have, as yet, been no reports of the formation of mixed-composition (Fe-Mg) olivine materials directly from the gas-phase at low (room) temperature. This has important implications for understanding dust compositions in lower temperature environments such as planetary/satellite atmospheres and the ISM.

Our earlier study (Saunders and Plane, 2006) was aimed at synthesising and studying the properties of nanomaterials as analogues of meteoric smoke particles or MSPs. This

paper extends our investigations to a more realistic 'tertiary' vapour system, whereby a mixture of iron, magnesium and silicon oxide vapours is generated, from which mixed composition olivine nanoparticles are produced. Electron microscope x-ray analysis (TEM-EDX) and electron energy loss spectroscopy (EELS) data from collected material is used to show that (1) the final particle composition is homogeneous and (2), the relative Fe/Mg composition in the particles can be controlled quantitatively from $x = 0 - 1$ by varying the relative flows of the organometallic precursors. To complement the laboratory studies, we use electronic structure theory to identify likely molecular structures and chemical pathways which result in the observed particle compositions.

2. Experimental Methods

An aerosol flow reactor system (cylindrical laminar flow glass cell fitted with a series of quartz windows which act as photolysis ports) described in detail previously (Saunders and Plane, 2006) was used for the nucleation and growth of refractory aerosol from the photo-oxidation of mixed vapours of the precursors, iron pentacarbonyl ($Fe(CO)_5$, 99.999%, Aldrich), magnesium ethoxide ($Mg(OC_2H_5)_2$, 98%, Aldrich) and tetraethyl orthosilcate or TEOS ($Si(OC_2H_5)_4$, 98%, Aldrich), in N_2 bath gas at 293 K and atmospheric pressure. Photolysis of the precursor vapours was achieved using a broad-band Xe arc lamp ($\lambda > 300$ nm), whose beam was directed through the quartz cell windows using a flat mirror, and attenuated using neutral density filters to achieve the desired photolysis rate in the experiments. A total gas flow rate (precursors, O_2 and N_2 bath gas) of 600 cm^3 per minute at STP was used in all experiments. Ozone ($10^{13} - 10^{14}$

136 cm^{-3}) was generated prior to addition to the aerosol flow reactor by passing the O_2 flow
137 through a small cell with a quartz window adjacent to a Hg pen lamp.

138 A series of particle production experiments was performed using varying ratios of the
139 three precursor vapours present in the reactor. The ratio was controlled experimentally by
140 varying the relative gas flow fractions of the entrained precursor vapours. Whilst vapour
141 pressure data for the Fe and Si liquid precursors has been reported in the literature
142 (Gilbert and Sulzmann, 1974; Alcott et al., 2004 respectively), no such data appears to
143 exist for the solid Mg precursor. In addition, all experiments were performed at constant
144 lamp irradiance in the flow reactor, corresponding to a calculated photolysis rate (J) of ~
145 2.0×10^{-4} s^{-1} for $Fe(CO)_5$ (determined from the wavelength-resolved lamp photon flux
146 and the molecular absorption cross-section – see Saunders and Plane, 2010). No cross-
147 section data is available in the literature for the other precursors. The generated particles
148 were sampled downstream of the flow cell by inertial deposition onto holey-carbon grids
149 (300 mesh Cu, Agar Scientific) suspended in the gas flow, for subsequent TEM (Philips
150 CM200) imaging and quantitative compositional analysis using energy dispersive x-ray
151 (EDX) and electron energy loss techniques.

152

153 **3. Results & Discussion**

154 3.1 Electron microscope and elemental analysis

155 Figure 1 is an electron micrograph of a particle aggregate generated by the photo-
156 oxidation of a mixture of the Fe, Mg and Si precursors described previously. Whilst the
157 maximum projected length of this structure from the 2D image is in excess of 2 microns,

158 it is evident that the fractal-like nature of the aggregate is generated from smaller particle
159 clusters made up of constituent 'primary' particles with an observable range of sizes
160 down to ~ 10 nm. Previous growth modelling analysis of iron oxide and silicate particles
161 generated within the same flow reactor (Saunders and Plane, 2006; 2010) indicate a
162 primary particle size typically between 6-8 nm for such particles under conditions of
163 room temperature and atmospheric pressure.

164

165 → **Figure 1**

166 Figure 2 shows EDX spectra obtained from particles generated from three different
167 vapour mixtures. The top spectrum was taken from a particle aggregate formed from the
168 photo-oxidation of the iron-silicon system, the middle spectrum from the iron-
169 magnesium-silicon system, and the bottom spectrum from the magnesium-silicon system.

170

171 → **Figure 2**

172

173 Seven different experiments were performed: one Fe/Si run, one Mg/Si run, and five
174 separate Fe/Mg/Si runs where the Fe and Mg precursor flows were varied. The relative
175 Fe, Mg and Si content in the particles was determined using the integrated EDX peak
176 areas and x-ray scattering cross-sections (Si_K, $Fe_{K,L}$ and Mg_K) (Goodhew et al., 2001).
177 Analysis was typically performed on 5 different regions of each sampled particle (using a
178 probe size of 1 nm), and on 5-10 different particles collected in the same experiment. The
179 elemental values obtained in this way were highly consistent, with less than 10%

180 variation for a given particle sample in each experiment. It should be noted that we did
181 not observe any particles of purely iron or magnesium oxide composition from these
182 experiments. The relative abundance data was then used to calculate values of $x_{particle}$ (=
183 Mg/(Mg+Fe)) for comparison with the olivine and pyroxene stoichiometries – $(Mg_xFe_{1-x})_2SiO_4$ and $Mg_xFe_{1-x}SiO_3$, respectively. These are listed in Table 1 along with the flow
185 rates used for the precursor species, oxidant and bath gas (N_2).

186

187 → **Table 1**

188

189 Figure 3 shows particle *x* values plotted against the ratio of (Mg+Fe)/Si for each
190 experiment. Within error, the average particle compositions from all experiments are
191 consistent with olivine and not pyroxene structures.

192

193 → **Figure 3**

194

195 For further verification of the particle compositions, electron energy loss spectroscopy
196 (EELS) was also conducted in order to quantify the oxygen content (O_K). These were
197 plotted as a ratio with respect to Fe, Mg and Si atomic content using the integrated peak
198 areas, as discussed in Saunders and Plane (2006), against the $x_{particle}$ values determined
199 above. Figure 4 indicates that the measured elemental data (coloured points) are in accord
200 with those predicted for olivine structures (solid coloured lines). In addition, as with our
201 earlier study, analysis of the $Fe_{L2,3}$ line structures (van Aken and Liebscher, 2002)

indicated a single (+2) oxidation state. Electron diffraction revealed no diffraction behaviour for any of the particle aggregates analysed at a number of different points and so confirmed that, for all samples, the particles were entirely amorphous.

→ **Figure 4**

The EDX/EELS analysis clearly indicates that particle composition resulting from the photo-oxidation of Fe-, Mg-, and Si-precursor vapours was homogeneous in all cases. From this, it can be concluded that particle nucleation in this system occurs from a homogeneous mix of condensable gas-phase species, the identities of which we will discuss in section 3.2.

If the Mg and Fe content in the particles are a fraction α of their respective gas-phase precursor concentrations i.e. Mg = $\alpha_{Mg}[Mg(OC_2H_5)_2]$ and Fe = $\alpha_{Fe}[Fe(CO)_5]$, then the ratio of Mg/Fe in the particle should be

$$\frac{Mg}{Fe} = \frac{\alpha_{Mg}[Mg(OC_2H_5)_2]}{\alpha_{Fe}[Fe(CO)_5]} \frac{216}{172} \quad \text{(I)}$$

α combines the precursor photolysis rate and efficiencies with which the resulting metal oxide and silicate condense. Note that in the case of $Mg(OC_2H_5)_2$ there does not appear to be published data on its photolysis cross section.

Since

$$x = \frac{\mathrm{Mg}}{\mathrm{Mg} + \mathrm{Fe}}$$

then

$$\left(\frac{x}{1-x}\right) = \frac{\alpha_{\mathrm{Mg}}\left[Mg(OC_2H_5)_2\right]}{\alpha_{\mathrm{Fe}}\left[Fe(CO)_5\right]}$$

Each vapour is entrained in a flow of N_2 passing through a reservoir cell containing its respective precursor. Under the slow flow conditions used here, the gas-phase precursor concentrations in the photolysis cell are then linearly proportional to the N_2 flows through their respective reservoir cells. Hence, the ratio of the precursor flows, f(Mg)/f(Fe), can be substituted into eqn. II, yielding

$$\left(\frac{x}{1-x}\right) = \frac{\beta_{\mathrm{Mg}} f(\mathrm{Mg})}{\beta_{\mathrm{Fe}} f(\mathrm{Fe})} \qquad \text{(III)}$$

where β combines α with the vapour pressure of the respective precursor (data on the vapour pressure of $Mg(OC_2H_5)_2$ does not appear to be available). Figure 5 is a plot of $x/(1-x)$ against f(Mg)/f(Fe), which is linear with a slope of 0.096 ($R^2 = 0.938$). Importantly, this demonstrates that the relative abundance of Mg to Fe in the particles has a linear dependence on the relative flows of their precursor vapours, so that particles with a composition anywhere between $x = 0$ and 1 can be made in a simple quantitative way.

→ **Figure 5**

3.2 Chemical pathways to final particle compositions

Photolysis of the precursor vapours produces Fe, Mg and Si atoms, and the reaction kinetics of these atoms and their oxides with O_2 and O_3 have been studied previously in our group (Gómez Martín et al., 2009a; Gómez Martín et al., 2009b; Helmer and Plane, 1994a; Rollason and Plane, 2000; 2001). Inspection of the rate coefficients listed in Table 2 shows that in the large excess of O_2 and O_3 employed in the present experiments, Fe and Mg would have been rapidly oxidized to FeO_3 and MgO_3, and Si to SiO_2

→ **Table 2**

In order to investigate the subsequent steps to particle formation, we now employ electronic structure calculations using the Gaussian 09 suite of programs (Frisch et al., 2009). The hybrid density functional/Hartree-Fock B3LYP method was employed together with the 6-311+G(2d,p) triple zeta basis set, which is a reasonably large, flexible basis set with both polarization and diffuse functions added to the atoms. The expected uncertainty in the calculated reaction enthalpies is ±20 kJ mol^{-1} at this level of theory. For each molecule the geometry was first optimised, and then vibrational frequencies calculated to determine the zero point energy correction. For the Fe-containing species, all possible spin multiplicities were investigated. The most stable isomers (invariably spin high), are reported here.

The present experiments were performed with a small excess of SiO_2 over the metal oxides (as in our previous study on Fe_2SiO_4 formation (Saunders and Plane, 2006)). Therefore, starting from the feedstock of MgO_3, FeO_3 and SiO_2 it is likely that the metal silicate molecules $MgSiO_3$ and $FeSiO_3$ first form via the following highly exothermic reactions:

$$MgO_3 + SiO_2 \rightarrow MgSiO_3 + O_2 \qquad \Delta H^o(0\ K) = -309\ kJ\ mol^{-1} \qquad (1)$$

$$FeO_3 + SiO_2 \rightarrow FeSiO_3 + O_2 \qquad \Delta H^o(0\ K) = -241\ kJ\ mol^{-1} \qquad (2)$$

As shown in Figure 6, these silicate molecules have planar kite-shaped geometries (the most stable electronic state of $FeSiO_3$ has quintet spin multiplicity i.e. four parallel unpaired electrons; $MgSiO_3$ is a singlet with no unpaired spins). A distinctive feature of the silicates is that they possess very large electric dipole moments: $\mu(MgSiO_3) = 12.2$ Debye and $\mu(FeSiO_3) = 9.5$ Debye. This will favour polymerization of the silicates, which should occur rapidly because of the long-range attractive forces generated between the polar molecules.

→ **Figure 6**

Figure 6 illustrates the geometries of the polymers formed between these silicates. The binding energies are extremely large:

287

288 $MgSiO_3 + MgSiO_3 \rightarrow (MgSiO_3)_2$ $\Delta H^o(0\ K) = -446\ kJ\ mol^{-1}$ (3)

289 $FeSiO_3 + MgSiO_3 \rightarrow FeSiO_3\text{-}\ MgSiO_3$ $\Delta H^o(0\ K) = -396\ kJ\ mol^{-1}$ (4)

290 $FeSiO_3 + FeSiO_3 \rightarrow (FeSiO_3)_2$ $\Delta H^o(0\ K) = -343\ kJ\ mol^{-1}$ (5)

291

292 Since the enthalpies for the addition of further silicate molecules to an embryonic particle
293 are likely to be similarly large, there is unlikely to be a free energy barrier to spontaneous
294 nucleation and growth.

295 However, the analysis of the particles formed in our experiments shows that they are
296 composed of olivines rather than pyroxenes. There are two likely ways in which this
297 happens. First, olivine molecules may actually form in the gas phase. This is because the
298 $MgSiO_3$ and $FeSiO_3$ molecules are produced in an excess of MgO_3 and FeO_3, so that the
299 following reactions can occur:

300

301 $MgSiO_3 + MgO_3 \rightarrow Mg_2SiO_4 + O_2$ $\Delta H^o(0\ K) = -252\ kJ\ mol^{-1}$ (6)

302 $MgSiO_3 + FeO_3 \rightarrow MgFeSiO_4 + O_2$ $\Delta H^o(0\ K) = -206\ kJ\ mol^{-1}$ (7)

303 $FeSiO_3 + MgO_3 \rightarrow MgFeSiO_4 + O_2$ $\Delta H^o(0\ K) = -273\ kJ\ mol^{-1}$ (8)

304 $FeSiO_3 + FeO_3 \rightarrow Fe_2SiO_4 + O_2$ $\Delta H^o(0\ K) = -221\ kJ\ mol^{-1}$ (9)

305

Once again, all these reactions are very favourable thermodynamically. The olivine molecules, which are illustrated in Figure 7, should also polymerize spontaneously through highly exothermic reactions. For example, for the two dimers shown in Figure 7:

$Mg_2SiO_4 + Mg_2SiO_4 \rightarrow (Mg_2SiO_4)_2$ $\Delta H^o(0\ K) = -512\ kJ\ mol^{-1}$ (10)

$MgFeSiO_4 + MgFeSiO_4 \rightarrow (MgFeSiO_4)_2$ $\Delta H^o(0\ K) = -529\ kJ\ mol^{-1}$ (11)

Figure 7 also shows the Mg_2SiO_4 tetramer, formed from the polymerization of two Mg_2SiO_4 dimers:

$(Mg_2SiO_4)_2 + (Mg_2SiO_4)_2 \rightarrow (Mg_2SiO_4)_4$ $\Delta H^o(0\ K) = -590\ kJ\ mol^{-1}$ (12)

→ **Figure 7**

This process is also extremely exothermic (calculated at the B3LYP/3-21+g level of theory), underlining the strong thermodynamic force behind polymerization of these molecules. Thus there is a plausible route involving reactions 1 and 2 to form the silicate molecules, followed by reaction 6 – 9 to form the olivine molecules, which would generate particles with the observed olivine structure where *x* would be equal to the relative rates of photochemical production of Mg to Fe atoms.

Note, however, that this reaction sequence requires reactions 6 – 9 to be faster than reactions 3 – 5 (where the silicates polymerize directly together). If in fact silicate polymerization is competitive, then the resulting amorphous pyroxene particles must rearrange internally to form olivines. This is the second way in which the observed olivine particles could form. To get a sense of the thermodynamic requirements for structural rearrangement, consider the enthalpies for the following reactions which convert pyroxene to olivine molecules:

$$MgSiO_3 + MgSiO_3 \rightarrow Mg_2SiO_4 + SiO_2 \qquad \Delta H^o(0\ K) = +57\ kJ\ mol^{-1} \qquad (13)$$

$$MgSiO_3 + FeSiO_3 \rightarrow MgFeSiO_4 + SiO_2 \qquad \Delta H^o(0\ K) = +36\ kJ\ mol^{-1} \qquad (14)$$

$$FeSiO_3 + FeSiO_3 \rightarrow Fe_2SiO_4 + SiO_2 \qquad \Delta H^o(0\ K) = +21\ kJ\ mol^{-1} \qquad (15)$$

The dimerization of SiO_2 is strongly exothermic:

$$SiO_2 + SiO_2 \rightarrow (SiO_2)_2 \qquad \Delta H^o(0\ K) = -401\ kJ\ mol^{-1} \qquad (16)$$

Hence, combining reactions 2×(13) + (10) + (16) gives:

$$4MgSiO_3 \rightarrow (Mg_2SiO_4)_2 + (SiO_2)_2 \quad \Delta H^o(0\ K) = -799\ kJ\ mol^{-1} \qquad (17)$$

and combining reactions 2×(14) + (11) + (16) gives:

346

347 $2MgSiO_3 + 2FeSiO_3 \rightarrow (MgFeSiO_4)_2 + (SiO_2)_2$ $\Delta H^o(0\ K) = -858\ kJ\ mol^{-1}$ (18)

348

349 Reactions 17 and 18 are therefore highly exothermic. This indicates that pyroxene might
350 rearrange into olivine in small particles by forming a separate SiO_2 phase. Of course, the
351 "separate phases" considered here only consist of dimers of olivine and silica molecules,
352 and further theoretical investigation in this direction would be extremely computer-
353 intensive. We therefore conclude that both direct formation of gas-phase olivine
354 molecules, and possibly some structural rearrangement of condensed silicates, play a role
355 under our experimental conditions.

356

357 3.3 Comparison with other laboratory studies of Mg-Fe-silicate formation

358 While the present study appears to be the first attempt to investigate the formation of
359 tertiary Mg-Fe-silicate meteoric smoke particles relevant to planetary atmospheres, there
360 have been a number of studies to investigate the formation of metal silicates under the
361 conditions of stellar outflow regions and the ISM. Replicating the conditions –
362 temperatures, pressures and timescales – of these environments in the laboratory is
363 challenging (Nuth et al., 2000). There have been essentially two types of experimental
364 approach. In the first, a sample of olivine, for example, is vaporized by flash heating
365 (Nagahara et al., 1988) or laser ablation (Brucato et al., 2002); the condensation products
366 of the resulting vapours are then collected and analysed. In the second type of
367 experiment, vapours of Fe, Mg and Si are produced in the presence of an oxidant by

368 decomposition of appropriate precursors, either photochemically (the present study) or in
369 a high temperature (500 - 1500 K) thermal reactor (Rietmeijer et al., 1999; Nuth et al.,
370 2000). This second type of experiment is designed to control the molecular "building
371 blocks" of the silicate particles, and here we will compare the results of the
372 photochemical and thermal systems. The experiments of Nuth and co-workers employed
373 the thermal decomposition of $Fe(CO)_5$ and SiH_4 in the presence of O_2 at a total pressure
374 of around 90 Torr (mostly made up of H_2). Magnesium atoms were added by vaporizing
375 Mg metal in a crucible within the thermal reactor. There are therefore two important
376 differences between the photochemical reactor used in the present study and the thermal
377 reactor: the use of O_3 versus O_2 as the oxidant; and a temperature of 293 K versus
378 temperatures typically above 1000 K, respectively. A further possibly significant
379 difference is that in the present experiment the three photolytic precursors are well-mixed
380 before entering the photolysis cell, whereas in the thermal reactor there must be some
381 spatial separation between the region where the Fe and Si precursors start to decompose
382 upon entering the hot region of the reactor, and the Mg vapour is produced from the
383 crucible.

384 The gas-phase chemistry in the two systems is somewhat different. In our photochemical
385 reactor, the building blocks of the metal silicates are FeO_3, MgO_3 and SiO_2, produced
386 under well-defined kinetic conditions (Section 3.2). In contrast, the chemistry in the
387 thermal reactor is quite complex. The metal dioxides FeO_2 and MgO_2 will form at the
388 relatively high pressure in the reactor:

389 $$Fe + O_2 (+M) \rightarrow FeO_2 \qquad (M = \text{mainly } H_2) \qquad (19)$$

390 $$Mg + O_2 (+M) \rightarrow MgO_2 \qquad (20)$$

Both these reactions have small barriers in their entrance channels so that, unusually for recombination reactions, their rate coefficients increase with temperature (Helmer and Plane, 1994b; Nien et al., 1993). The reactions forming the metal monoxides

$$Fe + O_2 \rightarrow FeO + O \quad (21)$$

$$Mg + O_2 \rightarrow MgO + O \quad (22)$$

are not competitive. The rate of reaction 21 (Akhmadov et al., 1988) only becomes equal to that of reaction 19 above 1500 K (at the pressure of the thermal reactor experiment). Although a rate expression for reaction 22 has been published (Kashireninov et al., 1982), this is clearly incorrect because the activation energy of 48 kJ mol^{-1} is much lower than the endothermicity of the reaction, ΔH_0 = 246 kJ mol^{-1} (Rollason and Plane, 2001). The upper limit to k_{22} must therefore be extremely small: e.g. $< 4 \times 10^{-21}$ cm^3 $molecule^{-1}$ s^{-1} at 1200 K. SiO will be produced by the decomposition of SiH_4 in O_2 (Gómez Martin et al., 2009a), but SiO_2 may then form via the reaction

$$SiO + O_2 \rightarrow SiO_2 + O \quad (23)$$

Since reaction 23 is only modestly endothermic (ΔH_0 = 63 kJ mol^{-1} (Gómez Martín et al., 2009b)), it may proceed at a rate similar to reactions 19 and 20 in the thermal reactor. Thus the main building blocks in the thermal reactor are FeO_2, MgO_2 and SiO and/or SiO_2.

A further complication in the thermal reactor is the decomposition of $Fe(CO)_5$ which occurs through sequential loss of CO. A reaction such as

$$FeCO + O_2 \rightarrow FeO_2 + CO \quad (24)$$

412 may be very fast, because the reaction is highly exothermic: ΔH_0 = -236 kJ mol^{-1},
413 calculated here at the B3LYP/6-311+g(2d,p) level of theory. Thus formation of Fe
414 silicate particles could occur at temperatures well below 1000 K once $Fe(CO)_5$ starts to
415 decompose, whereas the Mg silicates cannot not form until reaction 22 becomes fast
416 enough within the hot region of the reactor.

417 It is important to note that in spite of these differences in the molecular building blocks of
418 the two systems, olivine-type particles are produced in both cases. We have shown in
419 Section 3.2 that in the case of the photochemical reactor at low temperatures, the
420 production of olivine particles can be explained by the quenching from the gas phase of
421 molecules of olivine (or pyroxene). So this should be a kinetically controlled system,
422 where the ratio of Fe to Mg in the particles is controlled by the relative uptake rates of
423 their respective metal silicate molecules from the gas phase. In the thermal reactor
424 experiments, Nuth et al. (2000) observed the formation of pure magnesium silicate and
425 pure iron silicate amorphous grains above 1000 K. Strikingly, they did not observe any
426 mixed Fe-Mg particles with olivine composition. They attributed this surprising result to
427 the lack of eutectic compositions in the FeO-MgO phase diagram (Nuth et al., 2002). In
428 fact, thermodynamic considerations show that the condensation of particles from a Fe-
429 Mg-Si-O mixture under equilibrium conditions above 1000 K should produce mainly
430 pure forsterite (Mg_2SiO_4) and some enstatite ($MgSiO_3$) (Gail and Sedlmayr, 1999).
431 Although the initial polymerization may well be kinetically controlled, reactions such as

432 $$Fe_2SiO_{4(s)} + 2MgO_{2(g)} \rightarrow Mg_2SiO_{4(s)} + 2FeO_{2(g)} \quad (25)$$

433 where the Fe^{2+} ions are displaced by Mg atoms, are very exothermic (ΔH = -670 kJ mol^{-1},
434 calculated using ΔH = -157 kJ mol^{-1} for the reaction $Fe_2SiO_{4(s)} + 2Mg_{(g)} \rightarrow Mg_2SiO_{4(s)} +$

435 $2Fe_{(g)}$ (Gail and Sedlmayr, 1999), and ΔH = -256 kJ mol^{-1} for the gas-phase reaction
436 $MgO_2 + Fe \rightarrow FeO_2 + Mg$, calculated at the B3LYP/6-311+g(2d,p) level of theory). Thus
437 the thermal reactor results can be explained by the kinetic formation of mixed silicate
438 particles, subsequent displacement of Fe to form pure Mg silicates, and finally the
439 formation of Fe silicates once all the magnesium has been removed from the gas phase.
440 In contrast, in the low-temperature photochemistry system the composition of the
441 particles is frozen at the composition determined by the quenching kinetics, so that a
442 single solid phase is produced.

443

444 **4. Implications**

445 This new synthetic method for producing amorphous olivine nanoparticles is not
446 supposed to replicate the ambient conditions of either planetary atmospheres or oxygen-
447 rich stellar outflows. Nevertheless, some important conclusions can be drawn regarding
448 the formation of these particles in both types of environment. The rapidity with which the
449 particles form and grow in the laboratory, combined with the results of the electronic
450 structure calculations, suggests that particle formation is a spontaneous process i.e., there
451 are no free energy barriers to nucleation. Indeed, the long-range magnetic dipole forces in
452 Fe-containing particles which drive this rapid growth were explored by us in a previous
453 study (Saunders and Plane, 2006), where we showed that the rates of magnetic dipole-
454 controlled reactions actually get slightly faster at lower temperatures. Hence, particle
455 formation can be expected even at the very low temperatures of the ISM.

456 The pathway to particle formation in the photochemical reactor – formation of FeO_3,
457 MgO_3 and SiO_2 in the presence of O_3 and O_2 – is quite probably the route to forming
458 MSPs in the atmospheres of the terrestrial planets. The composition of MSPs in the
459 Earth's atmosphere has been a subject of speculation because their small dimensions both
460 precluded optical detection and also created major difficulties for direct rocket-borne
461 sampling and uncontaminated return from the mesosphere. However, there has been a
462 recent report of detectable particle extinction at two near-IR wavelengths at altitudes
463 above 50 km made from the AIM satellite (Hervig et al., 2009). Although this extinction
464 is consistent with refractive index data for the pyroxene structure $Mg_{0.4}Fe_{0.6}SiO_3$, new
465 work using additional wavelengths in the near-UV and near-IR indicates that the particles
466 have an olivine structure $Mg_{2x}Fe_{2-2x}SiO_4$, where $x \sim 0.5$ (unpublished data from M.
467 Hervig, presented at the 38th COSPAR General Assembly, Bremen, 2010). This is
468 consistent both with the results of the present study, and with the model prediction that
469 meteoric ablation produces roughly equal quantities of Fe, Mg and Si (Vondrak et al.,
470 2008). However, it should be borne in mind that since the formation of olivine particles
471 requires the condensation of Fe- and Mg- containing species with SiO_2, and all three are
472 trace species in the upper mesosphere (mixing ratios < 10 ppb), it is also likely that
473 meteoric vapours produce particles containing oxides such as Fe_2O_3 (Saunders and Plane,
474 2010a), and hydroxides and carbonates.

475 Regarding silicate grain formation in the ISM, the relevant precursor species in oxygen-
476 rich circumstellar outflows are thought to be MgO, FeO and SiO/SiO_2 (Gail, 2010; Gail
477 and Sedlmayr, 1999; Nuth et al., 2000), which at first glance are different from the
478 species in the photochemical reactor. However, FeO_3 and MgO_3 have the structures OFe-

479 O_2 and OMg-O_2 (Rollason and Plane, 2000; 2001), where the weakly-bound O_2 acts as a
480 chaperone to the metal oxide. Thus the chemistry in our system may not be very different
481 from that in the ISM. In any case, the fact that olivine-type particles are produced in the
482 photochemical and the thermal reactors (Section 3.3) implies that the precise nature of the
483 metal oxide is secondary.

484 Thermal reactor experiments (Nuth et al., 2000; Rietmeijer et al., 1999) demonstrate that
485 magnesium silicate (forsterite and enstatite) particles are the major product at high
486 temperatures (> 1000 K). This is in accord with observations of a high forsterite
487 abundance in the circumstellar dust shells of stars with high mass loss rates, where
488 nucleation and growth of silicate particles will be faster and thus occur at higher
489 temperatures (de Vries et al., 2010; Nuth et al., 2002). The results of the present study
490 should therefore be applicable to low mass loss rate stars, where condensation will be
491 slow enough that it mostly occurs in cooler regions. Indeed, there is experimental
492 evidence that Fe-rich olivines form at temperatures around 800 K (Nagahara et al., 1988),
493 which is consistent with the thermodynamic prediction that fayalite and ferrosilite should
494 condense below 900 K (Gail, 2010). Our experiments were carried out at 293 K and, as
495 explained above, there is no reason that the condensation of these species will not occur
496 even at very low temperatures. The formation of Fe-rich olivine particles in low mass loss
497 rate environments will have two important consequences. First, because condensation is
498 slower and the concentration of gas-phase species is continuously diluted in the outflow,
499 much smaller particles are likely to result. Second, the particles will almost certainly be
500 amorphous, as observed in the present study at 293 K. Annealing of Mg-Fe-silicates to
501 form crystalline olivines requires temperatures in excess of 1000 K (Nuth et al., 2002).

5. Conclusions

This paper describes a photochemical technique for generating amorphous olivine nanoparticles over a controlled composition range. Quantitative compositional analysis of the particles formed by the photo-oxidation of a mixture of Mg-, Fe- and Si-organometallic vapours in O_3 at room temperature is consistent with a range of olivine ($Mg_{2x}Fe_{2-2x}SiO_4$: $0 \leq x \leq 1$) structures. Starting from the known gas-phase chemistry of Mg, Fe and Si atoms in the presence of O_3 and O_2, which produces MgO_3, FeO_3 and SiO_2, we have used electronic structure calculations to elucidate the likely pathways to the formation of olivine particles: direct condensation of olivine molecules, and/or the condensation of metal silicates followed by solid-phase structural rearrangement into separate olivine and silica phases.

The observed preferential nucleation and growth of amorphous mixed-metal silicate particles from a suitable metal and silicon oxide gas-phase environment, indicates the likely *spontaneous* formation of such materials in any environment where iron and magnesium oxide molecules are present together with SiO_2 i.e. in planetary atmospheres where meteoric ablation occurs, and in cooler regions of the ISM, for example the gas outflows of low mass loss rate oxygen-rich stars.

Our photo-oxidation experiments, although not performed under realistic conditions (temperature and pressure) with respect to planetary atmospheres or the ISM, point to an efficient method for the production of nanoparticles of the composition and structure found in these environments.

524

525 **Acknowledgements**

526 This work was supported by funding from the UK Natural Environment Research
527 Council (grant NE/E005659/1).

528

529 **References**

530 Akhmadov, U. S., et al., 1988. Mechanism and kinetics of interaction of Fe, Cr, Mo, and
531 Mn atoms with molecular oxygen. Kinetics and Catalysis 29(2), 251-257.

532 Alcott, G.R., van de Sanden, R.M.C.M., Kondic, S., Linden, J.L., 2004. Vapor pressures
533 of precursors for the CVD of silicon-based films. Chem. Vap. Deposition 10, 20-22.

534 Brucato, J.R., Mennella, V., Colangeli, L., Rotundi, A., Palumbo, P., 2002. Production
535 and processing of silicates in laboratory and in space. Planet. Space Sci. 50, 829-837.

536 Colangeli, L., et al., 2003. The role of laboratory experiments in the characterisation of
537 silicon-based cosmic material. Astron. Astrophys. Rev. 11, 97-152.

538 de Vries, B. L., Min, M., Waters, L.B.F.M., Blommaert, J.A.D.L., Kemper, F., 2010.
539 Determining the forsterite abundance of the dust around asymptotic giant branch stars.
540 Astron. Astrophys. 516, A86, doi: 10.1051/0004-6361/200913588.

541 Dorschner, J., Begemann, B., Henning, Th., Jäger, C., Mutschke, H., 1995. Steps towards
542 interstellar silicate mineralogy. II. Study of Mg-Fe silicate glasses of variable
543 composition. Astron. Astrophys. 300, 503-520.

544 Draine, B.T., Lee, H.M., 1984. Optical properties of interstellar graphite and silicate
545 grains. ApJ. 285, 89-108.

546 Draine, B.T., 2003. Interstellar dust grains. Annu. Rev. Astron. Astrophys. 41, 241-289.

547 English, M.A., Lara, L.M., Lorenz, R.D., Ratcliff, P.R., Rodrigo, R., 1996. Ablation and
548 chemistry of meteoric materials in the atmosphere of Titan. Adv. Space Res. 17, 157-160.

549 Fast, K.E., et al., 2009. Comparison of HIPWAC and Mars Express SPICAM
550 observations of ozone on Mars 2006-2008 and variation from 1993 IRHS observations.
551 Icarus 203, 20-27.

552 Frisch, M.J., et al., 2009. Gaussian 09, Revision A.1, Gaussian Inc., Wallingford CT.

553 Gail, H.-P., 2010. Formation and evolution of minerals in accretion discs and stellar
554 outflows. Lect. Notes Phys. 815, 61-141.

555 Gail, H.-P., Sedlmayr, E., 1999. Mineral formation in stellar winds. I. Condensation
556 sequence of silicate and iron grains in stationary oxygen rich outflows. Astron.
557 Astrophys. 347, 594-616.

558 Gilbert, A.G., Sulzmann, K.G., 1974. Vapor pressure of iron pentacarbonyl. J.
559 Electrochem. Soc. 121, 832-834.

560 Goodhew, P.J., Humphreys, F.J., Beanland, R., 2001. Electron Microscopy and Analysis,
561 third ed. Taylor & Francis, London, 243 pp.

562 Gómez-Martín, J.C., Blitz, M.A., Plane, J.M.C., 2009a. Kinetic studies of
563 atmospherically relevant silicon chemistry. Part I: Silicon atom reactions. Phys. Chem.
564 Chem. Phys. 11, 671-678.

565 Gómez-Martín, J.C., Blitz, M.A., Plane, J.M.C., 2009b. Kinetic studies of
566 atmospherically relevant silicon chemistry. Part II: Silicon monoxide reactions. Phys.
567 Chem. Chem. Phys. 11, 10945-10954.

568 Gorny, S.K., Perea-Calderón, J.V., Garcia-Hernández, D.A., Garcia-Lario, P., Szczerba,
569 R., 2010. New groups of planetary nebulae with peculiar dust chemistry towards the
570 Galactic bulge. Astron. Astrophys. 516, A39, 10.1051/0004-6361/200913010.

571 Helmer, M., Plane, J.M.C., 1994a. Kinetic study of the reaction between Fe and O_3 under
572 mesospheric conditions. J. Chem. Soc. Faraday Trans. 90, 31-37.

573 Helmer, M., Plane, J.M.C., 1994b. Experimental and theoretical study of the reaction Fe
574 + O_2 + N_2 → FeO_2 + N_2. J. Chem. Soc. Faraday Trans. 90, 395-401.

575 Henning, T., 2010. Cosmic silicates. Annu. Rev. Astron. Astrophys. 48, 21-46.

576 Hervig, M.E., Gordley, L.L., Deaver, L.E., Siskind, D.E., Stevens, M.H., Russell III,
577 J.M., Bailey, S.M., Megner, L., Bardeen, C.G., 2009. First satellite observations of
578 meteoric smoke in the middle atmosphere. Geophys. Res. Lett. 36, L18805,
579 doi:10.1029/2009GL039737.

580 Hörst, S.M., Vuitton, V., Yelle, R.V., 2008. Origin of oxygen species in Titan's
581 atmosphere. J. Geophys. Res. 113, E10006, doi:10.1029/2008JE003135.

582 Hunten, D.M., Turco, R.P., Toon, O.B., 1980. Smoke and dust particles of meteoric
583 origin in the mesosphere and stratosphere. J. Atmos. Sci. 37, 1342-1357.

584 Ip, W.H., 1990. Meteoroid ablation processes in Titan's atmosphere. Nature 345, 511-
585 512.

586 Jäger, C., Dorschner, J., Mutschke, H., Posch, Th., Henning, Th., 2003. Steps towards
587 interstellar silicate mineralogy. VII. Spectral properties and crystallisation behaviour of
588 magnesium silicates produced by the sol-gel method. Astron. Astrophys. 408, 193-204.

589 Jäger, C., Molster, F.J., Dorschner, J., Henning, Th., Mutschke, H., Waters, L.B.F.M.,
590 1998. Steps towards interstellar silicate mineralogy. IV. The crystalline revolution.
591 Astron. Astrophys. 339, 904-916.

592 Jensen, A.G., Markwick-Kemper, F., Snow, T.P., 2008. Oxygen in the interstellar
593 medium. Rev. Mineral. Geochem. 68, 55-72.

594 Kashireninov, O. E., et al., 1982. Improvement of oxidation kinetic constants of alkali-
595 metal vapors. Zhurnal Fizicheskoi Khimii, 56(4), 1030-1031.

596 Kemper, F., Vriend, W.J., Tielens, A.G.G.M., 2004. The absence of crystalline silicates
597 in the diffuse interstellar medium. ApJ. 609, 826-837.

598 Kim, Y.H., Pesnell, W.D., Grebowsky, J.M., Fox, J.L., 2001. Meteoric ions in the
599 ionosphere of Jupiter. Icarus 150, 261-278.

600 Kimura, Y., Nuth III, J.A., 2007. What is the driving force to form refractory oxide
601 grains? Silicate spectra depend on their formation environment. ApJ. 664, 1253-1263.

602 Kotak, R., et al., 2009. Dust and the type II-plateau supernova 2004ET. ApJ. 704, 306,
603 doi:10.1088/0004-637X/704/1/306

604 Lavvas, P., Yelle, R.V., Vuitton, V., 2009. The detached haze layer in Titan's
605 mesosphere. Icarus 201, 626-633.

606 Li, A., Draine, B.T., 2001. On ultrasmall silicate grains in the diffuse interstellar medium.
607 ApJ. 550, L213-217.

McAuliffe, J.P., Christou, A.A., 2006. Modelling meteor ablation in the venusian atmosphere. Icarus 180, 8-22.

Migliorini, A., Piccioni, G., Cardesín Moinelo, A., Drossart, P., 2010. Hydroxyl airglow on Venus in comparison with Earth. Planet. Space Sci. in press.

Molina-Cuberos, J.G., López-Moreno, J.J., Arnold, F., 2008. Meteoric layers in planetary atmospheres. Space Sci. Rev. 137, 175-191.

Montmessin, F., et al., 2006. Subvisible CO_2 ice clouds detected in the mesosphere of Mars. Icarus 183, 403-410.

Nagahara, H., Kushiro, I., Mysen, B.O., Mori, H., 1988. Experimental vaporization and condensation of olivine solid solution. Nature 331, 516-518.

Nien, C. F., Rajasekhar, B., Plane, J.M.C., 1993. Unusual kinetic behaviour of the reactions $Mg+O_2+M$ and $Ca+O_2+M$ ($M = N_2$, He) over extended temperature ranges. J. Phys. Chem. 97, 6449-6456.

Noll, K.S., Roush, T.L., Cruikshank, D.P., Johnson, R.E., Pendleton, Y.J., 1997. Detection of ozone on Saturn's satellites Rhea and Dione. Nature 388, 45-47.

Nuth III, J.A., Hallenbeck, S.L., Rietmeijer, F.J.M., 2000. Laboratory studies of silicate smokes: Analog studies of circumstellar materials. J. Geophys. Res., 105(A5), 10387-10396.

Nuth III, J. A., Rietmeijer, F.J.M, Hill, H.G.M., 2002. Condensation processes in astrophysical environments: the composition and structure of cometary grains. Meteoritics Planet. Sci. 37, 1579-1590.

629 Pesnell, W.D., Grebowsky, J., 2000. Meteoric magnesium ions in the Martian
630 atmosphere. J. Geophys. Res. 105(E1), 1695-1707.

631 Plane, J.M.C., Helmer, M., 1995. Laboratory study of the reactions Mg + O_3 and MgO +
632 O_3: implications for the chemistry of magnesium in the upper atmosphere. Faraday
633 Discuss. 100, 411-430.

634 Rapp, M., Thomas, G.E., 2006. Modeling the microphysics of mesospheric ice particles:
635 Assessment of current capabilities and basic sensitivities. J. Atmos. Sol. Terr. Phys. 68,
636 715-744.

637 Rietmeijer, F.J.M., Nuth III, J.A., Karner, J.M., 1999. Metastable eutectic condensation in
638 a Mg-Fe-SiO-H_2-O_2 vapor: Analogs to circumstellar dust. ApJ. 527, 395-404.

639 Rietmeijer, F.J.M., 2002. The earliest chemical dust evolution in the solar nebula. Chem.
640 Erde. 62, 1-45.

641 Rollason, R.J., Plane, J.M.C., 2000. The reactions of FeO with O_3, H_2, H_2O, O_2 and CO_2.
642 Phys. Chem. Chem. Phys. 2, 2335-2343

643 Rollason, R.J., Plane, J.M.C., 2001. A kinetic study of the reactions of MgO with H_2O,
644 CO_2 and O_2: implications for magnesium chemistry in the mesosphere. Phys. Chem.
645 Chem. Phys. 3, 4733-4740.

646 Rosinski, J., Snow, R.H., 1961. Secondary particulate matter from meteor vapors. J.
647 Meteorol. 18, 736-745.

648 Saunders, R.W., Plane, J.M.C., 2006. A laboratory study of meteor smoke analogues:
649 Composition, optical properties and growth kinetics. J. Atmos. Sol. Terr. Phys. 68, 2182-
650 2202.

651 Saunders, R.W., Plane, J.M.C., 2010. The formation and growth of Fe_2O_3 nanoparticles
652 from the photo-oxidation of iron pentacarbonyl. J. Aero. Sci., 41, 475-489.

653 Self, D.E., Plane, J.M.C., 2003. A kinetic study of the reactions of iron oxides and
654 hydroxides relevant to the chemistry of iron in the upper mesosphere. Phys. Chem. Chem.
655 Phys. 5, 1407-1418

656 Thompson, S.P., Evans, A., Jones, A.P., 1996. Structural evolution in thermally
657 processed silicates. Astron. Astrophys. 308, 309-320.

658 Turco, R.P., Toon, O.B., Hamill, P., Whitten, R.C., 1981. Effects of meteoric debris on
659 stratospheric aerosols and gases. J. Geophys. Res. 86(C2), 1113-1128.

660 van Aken, P.A., Liebscher, B., 2002. Quantification of ferrous/ferric ratios in minerals:
661 new evaluation schemes of Fe L_{23} electron energy-loss near-edge spectra. Phys. Chem.
662 Minerals 29, 188-200.

663 Vondrak, T., Plane, J.M.C., Broadley, S., Janches, J., 2008. A chemical model of
664 meteoric ablation. Atmos. Chem. Phys. 8, 7015-7031.

665 Whalley, C.L., Plane, J.M.C., 2010. Meteoric ion layers in the Martian atmosphere
666 Faraday Discuss. in press.

667 Whittet, D.C.B., 2003. Dust in the Galactic Environment, second ed. IOP Publishing,
668 Bristol, 378 pp.

669 Williams, D.A., Taylor, S.D., 1996. The chemical role of cosmic dust. Q. J. R. Astr. Soc.
670 37, 565-592.

671 Williams, D.A., Hartquist, T.W., 1999. The chemistry of star-forming regions. Acc.
672 Chem. Res. 32, 334-341.

673 **Table 1** Flows (cm^3 min^{-1} at 293 K and 1 bar) used for the respective precursor vapours
674 (Fe-, Mg- and Si-) present in the particle formation experiments. Calculated atomic ratio
675 ($x_{particle}$ = Mg/(Mg+Fe)) from EDX analysis on particles collected from the respective
676 experiments is also shown.

677

Fe	**Mg**	**Si**	**O_2**	**N_2**	**Mg/Fe**	**$x_{particle}$**
15	0	100	40	445	0	0
11	20	100	40	429	1.82	0.11
9	40	100	40	411	4.44	0.36
6	50	100	40	404	8.33	0.47
3	75	100	40	382	25.0	0.65
3	100	100	40	357	33.33	0.78
0	50	100	40	410	-	1.0

678

679

680

681

682

683

684 **Table 2** List of the reactions and rate coefficients involved in the oxidation of Fe, to

685 FeO_3, Mg to MgO_3, and Si to SiO_2.

Reaction	***k*(293 K)** [a]	**Reference**
$Fe + O_3 \rightarrow FeO + O_2$	2.1×10^{-10}	Helmer and Plane, 1994a
$Fe + O_2 (+ N_2) \rightarrow FeO_2$	1.0×10^{-13}	Helmer and Plane, 1994b
$FeO + O_3 \rightarrow FeO_2 + O_2$	1.6×10^{-10}	Rollason and Plane, 2000
$FeO + O_2 (+ N_2) \rightarrow FeO_3$	9.5×10^{-11}	Rollason and Plane, 2000
$FeO_2 + O_3 \rightarrow FeO_3 + O_2$	2.5×10^{-10}	Self and Plane, 2003
$Mg + O_3 \rightarrow MgO + O_2$	1.4×10^{-10}	Plane and Helmer, 1995
$MgO + O_3 \rightarrow MgO_2 + O_2$	3.4×10^{-11}	Plane and Helmer, 1995
$MgO_2 + O_3 \rightarrow MgO_3 + O_2$	Not measured	See Plane and Helmer, 1995
$Si + O_2 \rightarrow SiO + O$	1.1×10^{-10}	Gómez-Martín et al., 2009a
$Si + O_3 \rightarrow SiO + O_2$	4.0×10^{-10}	Gómez-Martín et al., 2009a
$SiO + O_3 \rightarrow SiO_2 + O_2$	4.4×10^{-13}	Gómez-Martín et al., 2009b

686 [a] Rate coefficient at 293 K, units: cm^3 $molecule^{-1}$ s^{-1}

687

688

689

690

691

692 **Figure Captions**

693 **Figure 1** Transmission electron micrograph of a typical fractal-like particle aggregate
694 formed from a vapour mixture of Fe, Mg and Si precursors.

695 **Figure 2** EDX spectra of particles sampled from three particle production experiments in
696 which no Mg precursor vapour was present (top panel), no Fe precursor vapour was
697 present (bottom panel), and in which all three precursor vapours were present in the flow
698 reactor (middle panel). Characteristic element peaks are indicated at the respective
699 electron energy values.

700 **Figure 3** Plot of the measured elemental ratio (Fe + Mg)/Si in the sampled particles
701 against *x*, indicating an olivine [$(Mg_xFe_{1-x})_2SiO_4$] composition in all cases.

702 **Figure 4** Calculated element to oxygen ratios M:O (M = Fe (black data points), Mg
703 (blue) and Si (red)) from EELS analysis of particles from the same experiments as in Fig.
704 3, plotted against *x*. The solid lines (Fe is black, Mg is blue, Si is red) indicate the
705 relationships that would be expected for a pure olivine composition, and the dashed lines
706 those for pyroxene.

707 **Figure 5** Correlation plot of the ratio (*f*) of magnesium to iron precursor vapour flows
708 (Table 1) employed in the respective experiments against calculated atomic ratio (*x* =
709 Mg/(Mg+Fe)) in generated mixed silicate particles.

710 **Figure 6** Electronic structure calculations at the B3LYP/6-311+g(2d,p) level of theory of
711 the optimised geometries of $MgSiO_3$, $FeSiO_3$ and their dimers and mixed polymer.

712 **Figure 7** Electronic structure calculations of the optimised geometries of Mg_2SiO_4,

713 $MgFeSiO_4$ and Fe_2SiO_4; the dimers of Mg_2SiO_4 and $MgFeSiO_4$; and the Mg_2SiO_4

714 tetramer.

715

716

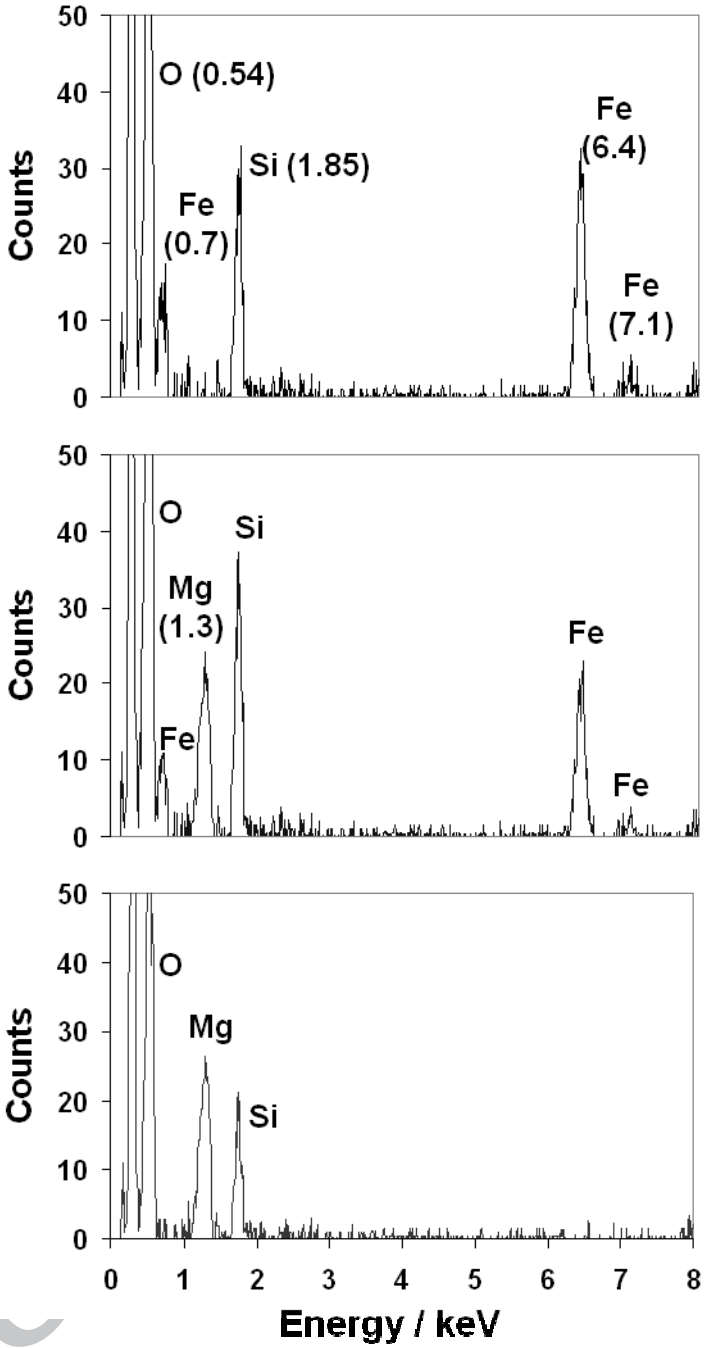

717

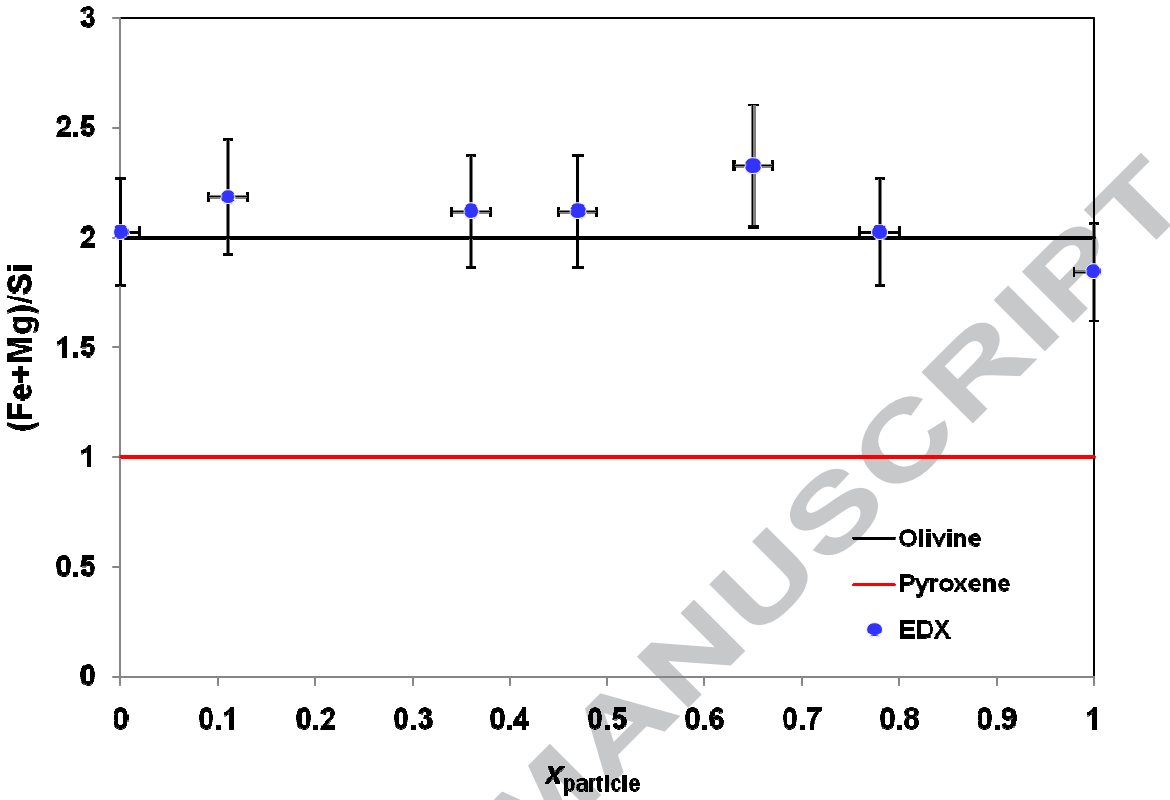

718

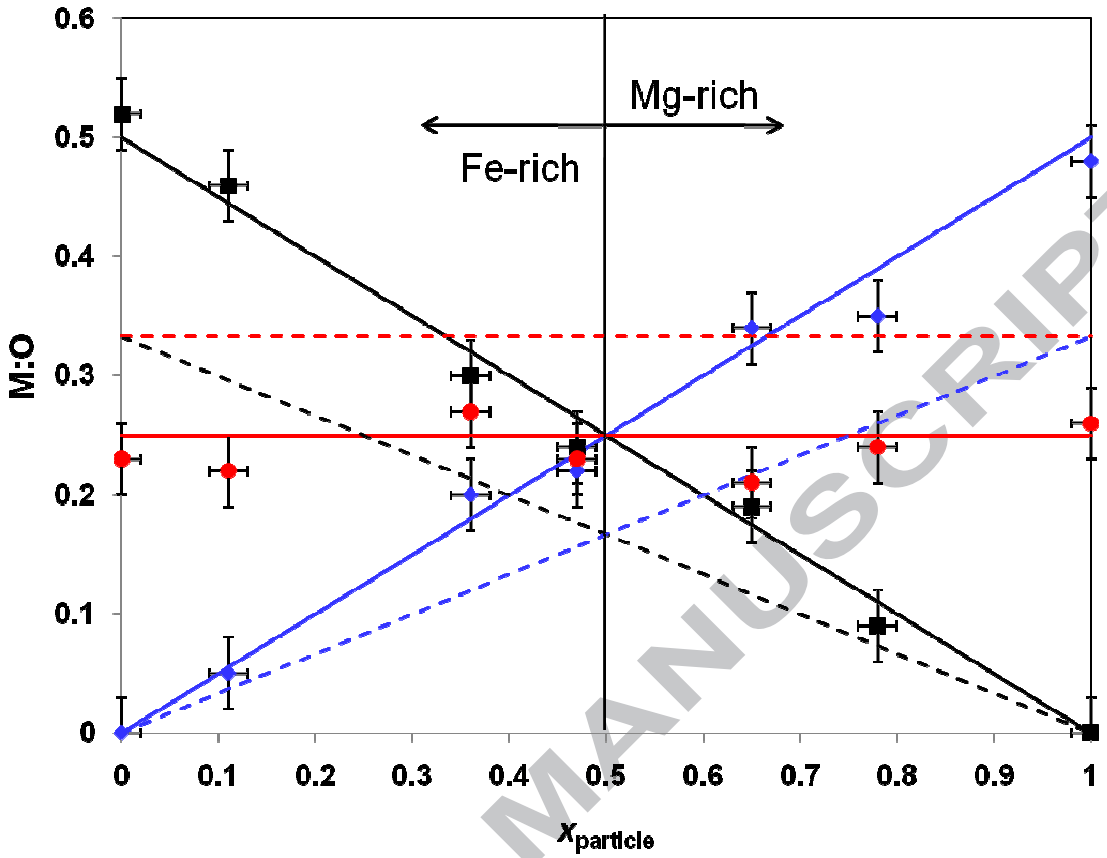

719

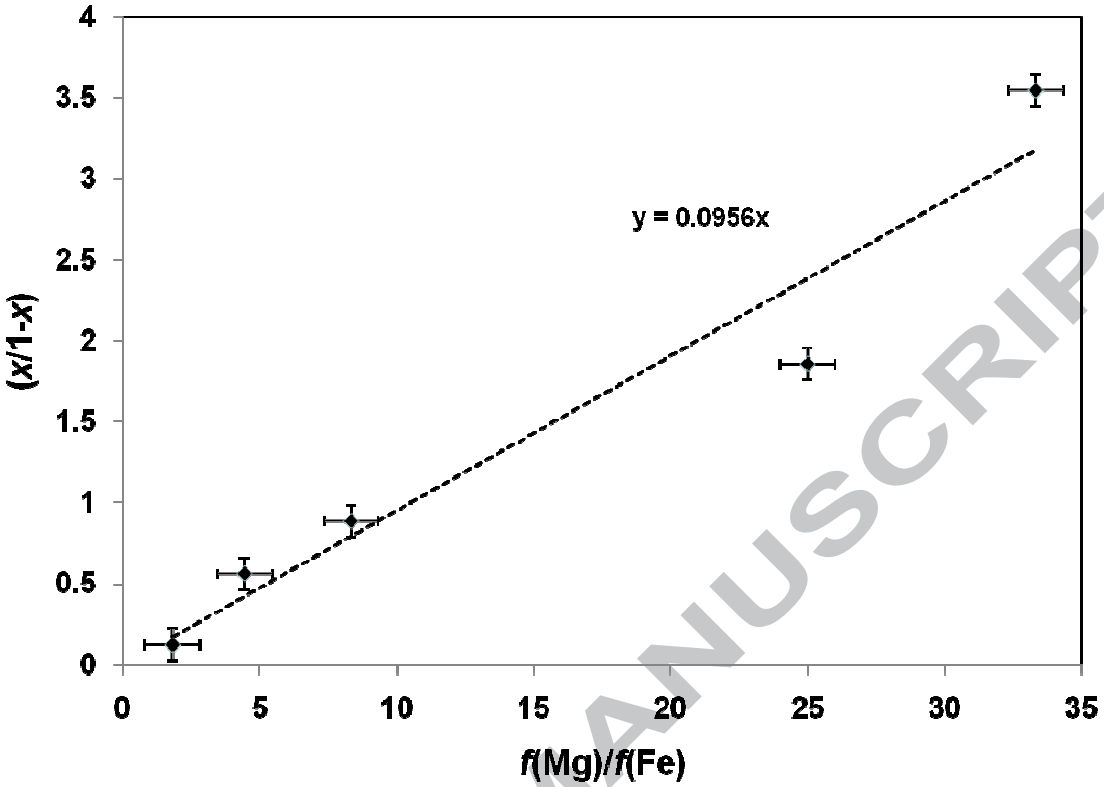

720

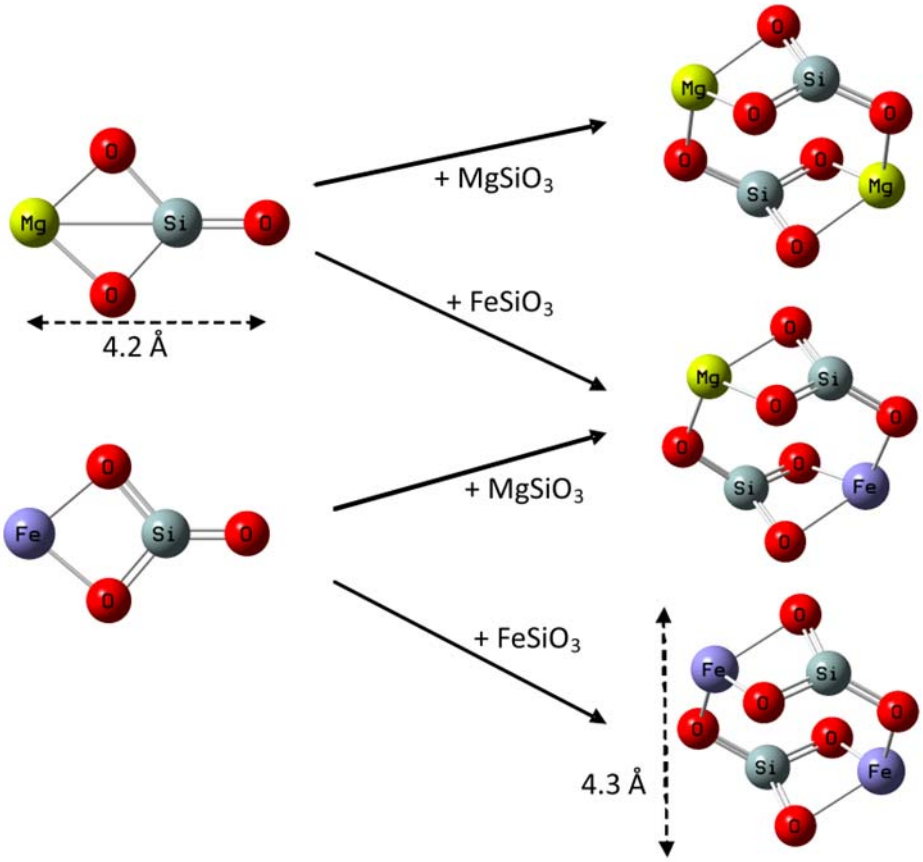

721

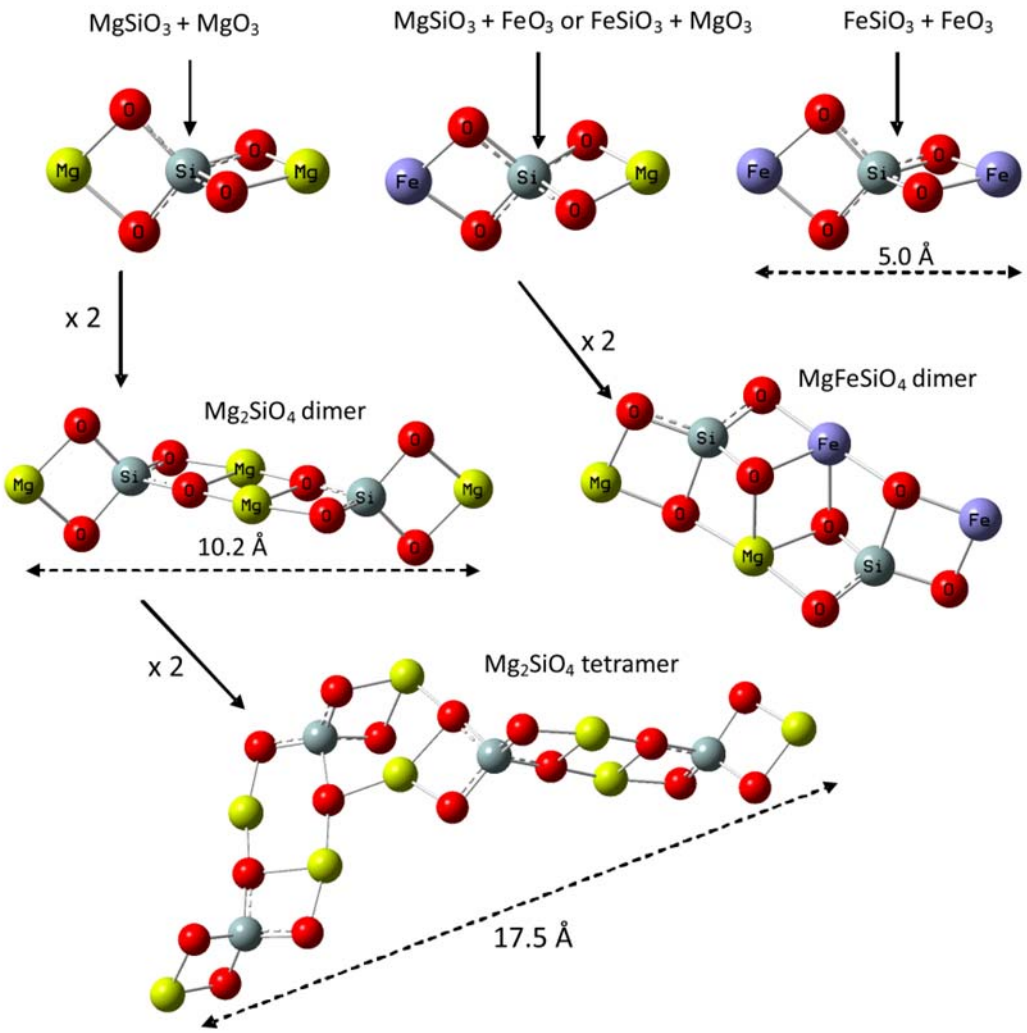

722

723